Control and Measurement of the Neutron-Gamma Ratio in Accelerator-based Neutron Fields

Yue Wang [a], Gang Guo [a], Qiming Chen [a], Jiancheng Liu [a], Qiaojuan Wang [a], Li Sui [a]*

[a]*Department of Nuclear Physics, China Institute of Atomic Energy, Beijing, China*

ARTICLE INFO

Article history:

Keywords:
Neutron field
Neutron-gamma ratio
Monte-Carlo simulation
Cyclotron applications

ABSTRACT

Research experiments regarding radiation effects demand the precise simulation of diverse radiation environments. In both the space and nuclear sectors, hybrid radiation fields with varying neutron-gamma ratios are prevalent. This study puts forward a convenient approach to regulate the neutron-gamma ratio and verifies its precision through experimental measurements at the 100MeV proton cyclotron of the China Institute of Atomic Energy. To achieve accurate and adjustable regulation of the neutron-gamma ratio within a range spanning from a few to several hundred, a neutron-gamma ratio regulator has been developed. The regulator was composed of different shielding materials with varying thicknesses and settled on the quasi-monoenergetic neutron beam line. The incident neutrons were generated by bombarding a lithium target with protons. Beam detection and calibration experiments were conducted, which demonstrated the effectiveness and superiority of generating hybrid radiation with adjustable neutron-gamma ratios in accelerator-based neutron fields.

1. Introduction

Hybrid neutron fields are commonly encountered in a wide array of nuclear scenarios, including nuclear facility operations, nuclear fuel production, spent fuel reprocessing, spaceflight, nuclear medical treatment, and so forth[1]. Neutrons are predominantly generated through nuclear reactions and thus typically exist in the form of a continuous energy spectrum, with gamma rays present concomitantly.

For example, in space, high-energy charged heavy ions and protons from Galactic Cosmic Rays and Solar Particle Events can trigger nuclear reactions with the shielding materials of spacecraft. These reactions result in copious amounts of secondary particles, such as neutrons and gamma rays within the space capsule. The energy spectrum of the neutrons is relatively broad, ranging from tens of keV to hundreds of MeV, while the gamma rays are primarily in the MeV energy range. According to available data, the radiation dose received during one day of flight in the space environment is approximately equivalent to the natural background external radiation dose on the ground for one year. Under the existing radiation shielding conditions, the radiation dose inside the International Space Station (ISS) for one year is about 170 mSv. During solar flare activities, the radiation dose can be even higher. Within the existing spacecraft shielding by materials like aluminium, the equivalent radiation doses contributed by secondary neutrons and gamma rays play a particularly important role, of which the contribution to the total equivalent dose for astronauts can approximately achieve more than 30%.

Extensive research has verified that neutron radiation can damage electronics, materials, and living organisms[2]. Epidemiological data has widely supported the notion that both neutron and gamma radiation can cause severe biological damage and lead to radiation-related occupational diseases. Currently, both domestic and international research communities have conducted investigations using gamma rays to evaluate radiation doses and assess damages within the radiation environments of the nuclear industry and manned space stations. Regarding neutrons, numerous studies have also been conducted. However, the relative biological effectiveness (RBE) of neutrons has not been definitively demonstrated, and existing findings indicate that the interaction mechanisms of neutrons with varying energies on living organisms differ significantly.

Despite the accomplishments achieved under conditions of single neutron or gamma-ray radiation, considering the unique operational settings in the nuclear industry and the radiation environments of space stations are characterized by the hybrid radiation fields where neutrons and gamma rays coexist, it remains crucial to conduct in-depth investigations into whether single-radiation simulations are equivalent to such mixed-radiation environments in terms of radiation biological effects. Mainstream research indicates that the biological effects of a neutron-gamma mixed field are not merely non-equivalent to those of individual radiation fields but are also related to the proportion of neutrons and gamma rays within it, which is the neutron-gamma ratio[3].

Since gamma rays are always present in a neutron field and the neutron-gamma ratio can contribute to the radiation effects, precise control of the ratio is vital for evaluating the radiation effectiveness of hybrid neutron fields with various parameters. This necessitates accurate adjustments and measurements of neutron-gamma ratios and their respective energy spectra. The measurement and discrimination technology for neutrons and gamma rays has been relatively mature[4-7].

Two dominant methods for generating neutron beam for sample irradiation include fission-based reactor technology and accelerator-based

* *Corresponding author：Li Sui.*
E-mail address: lisui@ciae.ac.cn:

proton targeting method. Earlier on, the neutron-gamma mixed fields are typically generated by nuclear fission reactors. Within the reactor, uranium-235, a fissile isotope of uranium, is bombarded with neutrons, resulting in the production of additional neutrons. These newly produced neutrons continue to collide with uranium-235, leading to the creation of even more neutrons. This so-called chain nuclear reaction establishes a neutron field which are then extracted through specific channels[8-9]. By employing neutron moderators and reflectors, the energy and angular distributions of the neutrons can be tailored for research into neutron-gamma simulation experimental techniques. Abroad, numerous studies have been conducted using the neutron-gamma mixed radiation fields generated by reactors[10-11]. For instance, aiming to meet the experimental requirements for simulating different radiation fields, Kelly et al. achieved the regulation of the neutron-gamma ratio within a 150-fold range on the SPR-III reactor[12]. Domestically, Li Junjie and others utilized lead as the main material for the neutron-gamma regulator, enabling the adjustment of the neutron-gamma ratio of the CFBR-II reactor radiation field within the range of 1.07×10^{12} - 4.87×10^{12} $cm^{-2}\cdot Gy^{-1}(Si)$[13].

However, reactors have several disadvantages, including complex structures, narrow neutron energy spectra, and large physical sizes. Consequently, the economic cost for biological effect research is relatively high, and experimental opportunities are quite limited. Thus, it is essential to develop more convenient experimental methods.

Another option, the accelerator-based proton targeting method involves accelerating protons to high-energy levels with accelerators and then directing protons to collide with a target material, thereby generating neutrons. Currently, lithium (^{7}Li(p,n)^{7}Be) and beryllium (^{9}Be(p,n)) targets are commonly used[14]. The reactions are as follows: $^{7}Li + p \rightarrow {}^{7}Be + n$ and $^{9}Be + p \rightarrow {}^{9}B + n$. When opting for a beryllium target, the proton energy must be at least 4 MeV to ensure sufficient neutron yield. However, beryllium is highly toxic, presenting significant operational risks. In contrast, the lithium target has a lower nuclear reaction threshold energy of 1.88 MeV, yields a higher number of neutrons, and provides good monochromaticity. Consequently, proton bombardment of lithium targets has become the preferred method for neutron production. Examples include Uppsala University in Sweden, UCL in Belgium, and the University of California-Davis in the United States, which all employ this method to generate neutrons[15-17]. In China, Tang Esheng et al. have utilized the 10-MeV proton linear accelerator at the Institute of High Energy Physics, Chinese Academy of Sciences, to produce neutrons with energies ranging from 2 to 5 MeV through target bombardment. Traditionally, this method has been solely a technique for neutron production, as the accompanying gamma rays are usually shielded[18]. However, if the accompanying gamma rays are not shielded, it transforms into a promising method for generating a neutron-gamma mixed radiation field. This method has several benefits, such as ease of operation, low economic cost, a wide neutron energy spectrum, rapid adjustment of the neutron-gamma ratio, and increased experimental time[19].

At China Institute of Atomic Energy (CIAE), which operates a 100MeV proton cyclotron, a quasi-monoenergetic neutron beamline (S1 branch line) and a white light neutron irradiation branch line (S2 branch line) have been implemented. In this study, we employed a regulator design using Monte-Carlo simulation, which integrates two materials of different atomic numbers to adjust neutron and gamma yields during proton irradiation. Furthermore, the lithium target has been tailored to match the cross-sections for nuclear reactions with proton beams of varying energies. For neutron measurements, plastic scintillator detectors [20]and ^{238}U fission chambers were used, while the PTW UNIDOS standard ionization chamber and dosimeter were utilized for gamma measurements. Additionally, the custom-designed collimator, shielded bunkers, and extended lengths of electric cables allow for the positioning of electronic devices at a safe distance from the irradiation area. The experimental setup substantially reduces the risk of radiation damage and minimizes noise interference from the accelerator.

2. Materials and methods

2.1. Quasi-monoenergetic neutron source

The study utilized the S1 branch line of the 100 MeV proton cyclotron, where high-purity proton beams can be accelerated to energies ranging from 70 to 100 MeV and flow strengths up to 520 μA. After passing through a series of transport devices, including deflection magnets, the protons are directed into the target chamber within the shielded area to bombard a lithium target, producing neutrons through nuclear reactions.

The ^{7}Li(p,n)^{7}Be reaction offers the highest intensity and the most monochromatic neutron source available, and it is the sole quasi-monoenergetic neutron source capable of energies up to 500 MeV. Based on experimental data regarding nuclear reactions, the characteristics of the neutron field resulting from protons colliding with a ^{7}Li target are dependent on the proton energy. The reaction energy of the ^{7}Li(p,n)^{7}Be reaction is -1.646 MeV, and the threshold energy for neutron production is 1.881 MeV. Consequently, with incident proton energies ranging from 1.9 to 2.4 MeV, the ^{7}Li(p,n)^{7}Be reaction yields only the ground state ^{7}Be, that is, ^{7}Li(p,n_0)^{7}Be, and the resulting neutron is mono-energetic with a very large cross section (300-500 mb). When the proton energy surpasses 2.4 MeV, the resultant ^{7}Be can be excited to its first excited state (0.43 MeV), resulting in the simultaneous occurrence of ^{7}Li (p,n_0)^{7}Be and ^{7}Li (p,n_1)^{7}Be reactions. When the proton energy is relatively small, the proportion of n_1 is less than 10%. At this juncture, the neutrons can still be considered quasi-monoenergetic. Furthermore, protons with energies exceeding 3.68 MeV can initiate the ^{7}Li (p,n^{3}He)^{4}He reaction channel, a three-body reaction that yields neutrons in a continuous energy spectrum, with energies below the mono-energetic peak. Protons above 7.06 MeV excite ^{7}Be to its second excited state (4.55 MeV), and even higher proton energies can excite ^{7}Be to its third and fourth excited states. An additional increase in proton energy opens further reaction channels, such as ^{7}Li(p,2n)^{6}Be. In brief, the n_0 and n_1 neutrons produced by the reactions ^{7}Li(p,n_0)^{7}Be and ^{7}Li(p,n_1)^{7}Be basically form the mono-energetic peak of the quasi-monoenergetic neutron spectrum resulting from the p→^{7}Li reaction. In contrast, neutrons from other reaction channels constitute the continuous spectrum of neutrons with energies below the mono-energetic peak[21].

Regarding angular distribution, the ^{7}Li(p,n)^{7}Be reaction cross-section for $n_{0,1}$ neutrons is primarily concentrated in the 0° direction. It initially increases with the incident proton energy and then stabilizes around 35 mb for incident protons ranging from 70 to 100 MeV. The neutron fluence rate of the mono-energetic peak exiting in the 0° direction can be calculated using the following equation:

$$\Phi_{\theta=0}(n_{0,1}) = \sigma_{\theta=0}(n_{0,1}) \times \Phi_p \times \rho_{^7Li} \times d_{^7Li} \quad (1)$$

Where $\sigma_{\theta=0}(n_{0,1})$ is the cross section in the 0° direction, Φ_p is the incident proton flow intensity, ρ_{7Li} is the atomic density of the ^{7}Li target, and d_{7Li} is the thickness of the ^{7}Li target.

In the 0° direction, the production cross section for quasi-monoenergetic neutrons is considered to be 35 mb/sr, the atomic density of the lithium target is 2.541×10^{22}/cm^3, and the thickness of the lithium target is denoted as d mm, with a ^{7}Li abundance of 92.5 percent and a ^{6}Li abundance of 7.5 percent. The proton flow intensity is denoted as A μA, and the number of protons per unit time incident on the lithium target is calculated as $A/(1.6\times10^{-19})$. Thus, the flux rate of quasi-monoenergetic neutrons produced during 70-100 MeV protons bombarding the lithium target can be theoretically calculated.

From the calculated data, the relationship between the energy and flow intensity of the incident proton and the resulting neutron flux rate can be derived. Ultimately, thicknesses of 4mm and 6mm were chosen for the lithium target to satisfy the requirements for proton incidence at various energies. Also, spatial position distribution of the lithium target was subsequently designed to match the dose rate required for the experiment. Notably, the lithium target is prone to oxidation and must be installed in an inert atmosphere within a glove box during the installation process.

2.2. Design and optimization of the regulator

In this study, the Geant4 software was utilized to simulate the effects of various materials on neutron-gamma ratio modulation. Geant4, a Monte Carlo software package developed by CERN (European Organization for Nuclear Research), is capable of simulating the physical transport of particles in matter using a multitude of complex physical models. It is not only used to simulate the interactions of common elementary particles but also to model particles with a broad energy spectrum, ranging from keV to GeV. Geant4 also provides the NDL (Neutron Data Library) cross section database, which encompasses various neutron reaction cross sections, including elastic scattering and capture, among others. Furthermore, Geant4 boasts an extensive database of interactions involving high-energy particles and rays. The theoretical simulation research on neutrons and gammas based on Geant4 is quite abundant[22-23].

Initially, in Geant4, a quasi-monoenergetic neutron source was simulated in the same way of bombarding a lithium target with a 100MeV proton beam. Subsequently, using this neutron source as the incident particle source, the shielding effects of heavy-element and light-element materials on neutrons and gamma rays, as well as the attenuation relationship with the shielding thickness, were calculated separately[24]. According to recent research, six different materials—lead (Pb), tungsten (W), aluminum (Al), graphite (C), water, and polyethylene—were initially selected as shielding bodies for the study[25]. By analyzing the neutron spectra and the yields of secondary particles (such as gamma rays) after passing through the shielding bodies, and in light of practical application requirements, lead and polyethylene were chosen as the primary materials for the neutron-gamma ratio regulator. After the materials' determination, combination models of lead and polyethylene with thickness gradients were created as a preliminary model of the neutron-gamma ratio regulator. In Geant4 spatial layout setting, the quasi-monoenergetic neutron beam reached the target area to interact with the regulator model after passing through the collimator, which can completely block the escaping neutrons. A detector and scoring model was set up at a certain distance behind the regulator. By evaluating the yields and spatial distributions of neutrons and gamma rays at the detector region, the performance of the regulator to adjust the neutron-gamma ratio was examined.

Based on theoretical simulations, the physical regulator was designed and manufactured. Various shielding bodies were installed on the experimental platform, which could be combined remotely via remote control of a pneumatic system. An air compressor was selected as the power source, with all the regulator components connected through an air circuit for power control. This setup prevents malfunctions of traditional motor-driven systems in high-radiation environments, ensuring the operational stability and reliability of the neutron-gamma ratio regulator.

Accelerator experiments were then conducted to verify the gap between the regulator's actual adjustment capabilities and the theoretical simulations, and targeted optimizations were subsequently performed.

2.3. Experimental arrangement

Utilizing the proton cyclotron at CIAE, a 100 MeV proton beam, after tube transport, was directed onto a 6 mm lithium target, while an 80 MeV proton beam current was directed onto a 4 mm lithium target to generate quasi-monoenergetic neutron beams with their respective energies. The proton beam flow intensity in front of the target was measured at 1.4 μA, and the proton current intensity through the Faraday tube after the deflection magnet was measured to be between 0.8-0.85 μA, which corresponds to approximately 60% proton transport efficiency.

The neutron-gamma ratio regulator was positioned after the deflector magnet and before the collimator. It comprises 5 pieces of lead and 1 piece of polyethylene, with the following thicknesses: 1.6 cm (lead), 0.8 cm (lead), 0.4 cm (lead), 0.2 cm (lead), 0.1 cm (lead), and 1 cm (polyethylene). The regulator is operated by a pneumatic device, which includes an air circuit and an air pump, allowing for 2^6=64 different thickness combinations that can all be remotely switched.

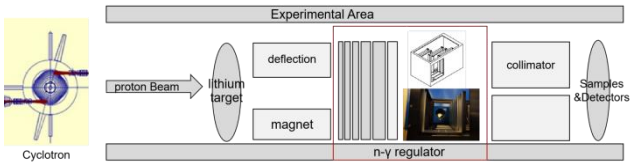

Fig. 1 Design and Physical Drawing of the n-γ Ratio Regulator

The metal collimator, embedded within the shielding concrete wall, allows only a circular beam within a radius of 5 cm to pass through. Subsequently, the detector and sample irradiation rig were established, utilizing a plastic scintillator detector and a ^{238}U fission chamber for neutron measurements, as well as a PTW UNIDOS standard ionization chamber and dosimeter for gamma measurements.

During quasi-monoenergetic neutron irradiation at varying energies, the moderator's combination mode was altered to achieve neutron attenuation through materials of differing thicknesses. The corresponding neutron-gamma ratios were then analyzed to verify the efficacy of accelerator-based neutron-gamma mixed field generation.

2.4. Neutron and gamma measurement

The ^{238}U fission chamber detects neutrons by utilizing the fission fragments resulting from the interaction of neutrons with heavy nuclei,

which ionize gas atoms within the gas chamber and then generate signals. The high kinetic energy (~160 MeV) of the fission fragments ensures a high ionization efficiency, leading to large output pulse amplitudes and a strong resistance to gamma background and electronic noise.

Practically, the fission chamber can function as an absolute measurement device for neutron flux rates. However, the measurement environment often contains scattered background neutrons with energies around 1 MeV, and the ^{238}U fission chamber inevitably includes nuclides such as ^{234}U and ^{235}U, which have large fission cross-sections for low-energy neutrons. This results in a high recorded pulse count. Consequently, to scale an absolute neutron measurement, it is essential to use a plastic scintillator detector in conjunction with the ^{238}U fission chamber.

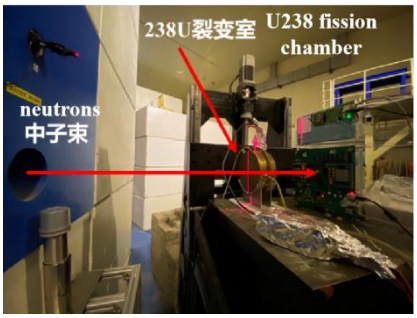

Fig. 2 Measurement of quasi-monoenergetic neutron injection using the ^{238}U fission chamber

Real-time diagnostic measurements of gamma radiation were conducted online using a UNIDOS dosimeter and a 0.6 cc gamma standard ionization chamber, as depicted in Fig. 3. The gamma dose data can be accessed in real time via remote data transmission. Throughout the test, the dosimeter was secured at a location 0.8 meters from the exit of the collimator, and the physical layout of the site is illustrated in Fig. 3 c.

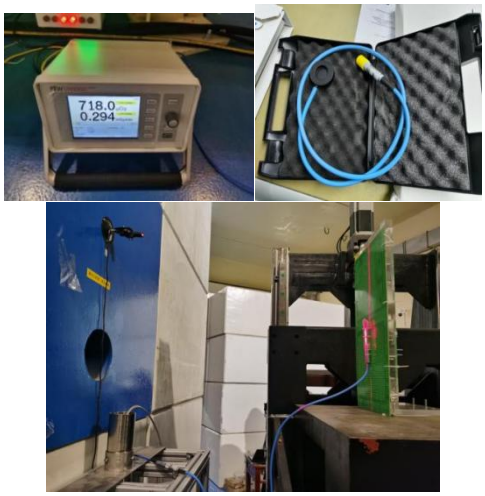

Fig. 3 (a) Gama Dosimeter, (b) PTW Standard Ionization Chamber and (c) Gamma Measurement Site

3. Results

3.1. Generation and measurement of a quasi-monoenergetic neutron beam

According to Eq.1, quasi-monoenergetic neutron beams generated by proton bombardment of lithium targets of varying thicknesses can be computed, and subsequently, their attenuation in air can be calculated using a Monte Carlo program Geant4. For a lithium target with a thickness of 4 mm, the theoretical quasi-monoenergetic neutron flux rate at the exit of the collimator (located 5.3 meters from the target) is 0.73E4 $cm^{-2}s^{-1}$ when the proton current is 1 μA. At the standard irradiation position, which is 6.1 meters from the target, the flux rate should be 0.55E4 $cm^{-2}s^{-1}$.

As for the experimental measurement, ^{238}U fission chamber utilizes natural uranium with an effective area diameter of 100 mm and a thickness of 560 μg/cm². Argon-methane gas (90% Ar + 10% CH4) serves as the ionization medium. In natural uranium, the nucleon ratio is 99.2647% for ^{238}U, 0.7295% for ^{235}U, and 0.0058% for ^{234}U. Consequently, the total uranium content in the ionization chamber amounts to 43.982 mg, with a thickness of 29.551 μm, a nucleon density of $4.794 \times 10^{22}/cm^3$, and a total number of nuclei at 1.113×10^{20}. The respective numbers of nuclei for ^{238}U, ^{235}U, and ^{234}U are 1.104×10^{20}, 8.117×10^{17}, and 6.453×10^{15}.

Without the regulator, quasi-monoenergetic neutrons were produced by bombarding a target with 100 MeV protons at a current of 120 nA, after passing through 4 mm lithium. The ^{238}U fission ionization chamber was positioned 6.1 meters from the lithium target, ensuring the neutron beam fully covered the effective area of the ^{238}U.

The neutron flux rate was measured, with the irradiation measurement time lasting 1688 seconds. The fission spectrum obtained is shown in Fig. 4, and the count above the screening threshold was 4198, which corresponds to a count rate of 2.487/s.

The injection rate of neutrons at the measurement point is:

$$\varphi = \frac{N_f}{\sum_i N_i \sigma_i^f} K \tag{2}$$

Where N_i represents the number of nuclei for ^{238}U, ^{235}U, and ^{234}U; σ_i^f is the U(n, f) cross section ($10^{-24}cm^2$), with neutron fission cross section data sourced from ENDF/B-VIII; K is the total correction factor, using data from the literature, with an average value of 0.2288, which corrects for the largest factor, the correction of low-energy neutrons, and the chosen parameter from the literature is 0.2057.

After calculation, the quasi-monoenergetic neutron injection rate was measured to be 5.1×10^2 $cm^{-2}s^{-1}$, which is close to the theoretical value of 6.6×10^2 $cm^{-2}s^{-1}$. Given that low-energy neutrons below the screening threshold are inherently disregarded in fission chamber measurements, the measured value is, by definition, smaller than the theoretical value.

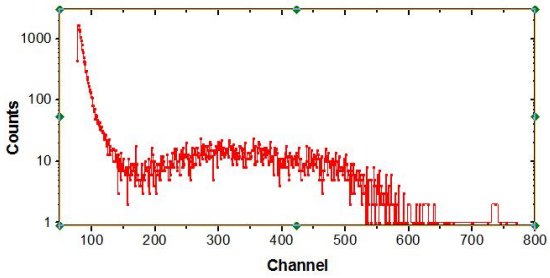

Fig. 4 Quasi-Monoenergetic Neutron Fission Spectrum

3.2. Theoretical possibilities for controlling the neutron gamma ratio

In Geant4, neutrons of varying energies were utilized as an incident particle source to analyze the effect of diverse materials with varying thicknesses on the neutron-gamma ratio regulation capabilities. The results demonstrate that the neutron-gamma ratios of different materials predominantly exhibit a similar trend of decreasing with the increase of material thickness. For high-Z materials, as the thickness of the material increases, the neutron yield initially rises and subsequently falls. In contrast, for low-Z materials, an increase in thickness leads to a continuous decline in neutron yield. Generally, the overall neutron yield tends to be below 1. It is evident that high-Z materials can be used to enhance the neutron yield when they reach a certain thickness, whereas low-Z materials can be utilized to reduce the neutron yield. In lead and tungsten, the gamma yield reaches its peak at the thickness of 3 cm. In other materials, it continues to increase as the thickness grows. The gamma yield of metallic materials is significantly higher than that of non-metallic materials. Most of the gamma yield is concentrated in the energy range below 6 MeV.

Among the six different materials, the neutron-gamma ratios of high-Z materials exhibit a more moderate trend, such as those of tungsten and lead materials between 8 and 13, and those of aluminium between 8 and 40; whereas the low-Z materials possess a larger range of adjustability. The neutron gamma ratios of graphite (20-144), water (42-236), and polyethylene (57-374) exhibit this characteristic. The combination of different materials and thicknesses allows for the quasi-continuous variation of the neutron gamma ratio from a few to several hundred, thereby enabling the large-scale adjustment of the neutron gamma ratio. Following comprehensive consideration of economic cost and processing difficulty, it was determined that lead would be the optimal gain material for the regulator's neutron and gamma yield, while polyethylene was selected as the gain material for the neutron yield.

The thickness gradient of metallic lead is further divided to simulate the distribution of a 100 MeV neutron energy spectrum. The results indicate that as the thickness of the lead material increases, the neutron yield in the low-energy region gradually rises, while the neutron yield in the middle and high-energy regions initially increases and then decreases. Consequently, the proportion of neutrons in the lossless region (100 MeV) gradually diminishes. At a lead material thickness of 20 cm, the lossless neutron yield is only 0.278, indicating the existence of a thickness threshold at which the gain effect of lead on neutron yield is maximized. This suggests that there is an optimal thickness for lead to enhance neutron yield.

Further simulation of the neutron and gamma yield as the thickness of the lead material changes is necessary. As the thickness of the lead material increases, the neutron and gamma yield initially rise and then fall. At a thickness of 4 cm, the neutron yield peaks at 1.217, and the gamma yield is 0.136, resulting in a neutron-gamma ratio of approximately 8.925. At a thickness of 5 cm, the neutron yield is 1.211, and the gamma yield reaches its maximum of 0.925. This indicates that there is a thickness threshold for lead to achieve the highest neutron yield. In the design of a neutron-gamma ratio regulator, a lead thickness of 4 cm was chosen to maximize neutron yield, while a thickness of 5 cm was selected to maximize gamma yield.

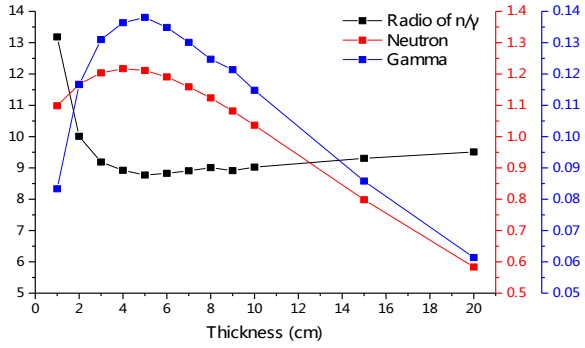

Fig. 5 Neutron and gamma yields and ratios for 100 MeV neutrons passing through different thicknesses of lead

In the context of the minimum neutron-gamma ratio, the thickness of the fixed lead is set at 4 cm, with the potential for polyethylene thickness ranging from 1 to 9 cm. The polyethylene can be utilized to effect minor alterations in neutron and gamma yields, as well as the neutron-gamma ratio distribution. The simulation results demonstrate that the placement of the polyethylene material in front of the 4 cm-thick lead material exerts a discernible influence on the middle and high-energy segments of the neutron energy spectrum. With an increase in polyethylene thickness, there is an observed rise in the percentage of neutron yield in the 80-100 MeV energy range, accompanied by a gradual decline in the percentage of neutron yield in the 100 MeV no-loss region. This suggests that the polyethylene material enhances the reaction cross section of the neutron, leading to a reduction in the percentage of lossless neutrons in the 80-100 MeV energy interval. Consequently, the percentage of neutrons decreases.

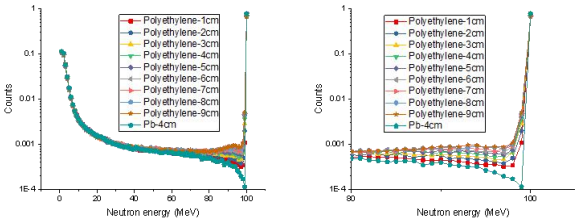

Fig. 6 Neutron energy spectra of 100 MeV neutrons passing through different thicknesses of polyethylene and lead (a)total energy spectrum, (b) 80 - 100 MeV local energy spectrum

It is shown that as the thickness of polyethylene increases, the neutron and gamma yield decrease slightly but consistently, resulting in the neutron-gamma ratio remaining relatively unchanged. This trend can be attributed to the neutron yield of a specific thickness of polyethylene being approximately equal to that of lead, while the gamma yield of lead is several times higher than that of polyethylene. Consequently, the contribution of polyethylene's gamma yield is almost negligible, and its neutron-gamma ratio is predominantly influenced by the lead material. However, this adjustment can be made for the fine tuning of the neutron-gamma ratio. For example, in the specific instance of the combination of 1-9 cm polyethylene and 4 cm lead, the neutron-gamma ratio can be meticulously calibrated within the range of 8.83 to 9.03.

When addressing a high neutron-gamma ratio, setting the polyethylene thickness to 1 cm may stabilize the neutron yield. As the thickness of the small-scale lead increases, both neutron and gamma yields gradually rise. However, the increase in gamma is significantly larger than that of the neutron, leading to a reduction in the neutron-gamma ratio. It is clear that by adjusting the thickness of the lead, the neutron-gamma ratio can be varied from 300 to 9.9. Evidently, altering the thickness of lead allows for fine-tuning of the neutron-gamma ratio from 300 to 9.9 to meet the requirements of changes in the large-scale neutron-gamma mixed radiation field.

3.3. Measurement of the neutron-gamma ratio

The measurement of the neutron-gamma mixed field, produced by the interaction of a 6 mm lithium target with a 100 MeV proton beam, was conducted on the S1 branch line of 100 MeV proton cyclotron at CIAE. The measurement process involved the utilization of a neutron-gamma ratio regulator, and the resulting result is presented as follows.

The analysis revealed an short increase in both neutron flux and gamma dose rate at the lead thickness of 0.1 cm. However, this trend was followed by a subsequent decrease in both measures as the lead thickness increased. The neutron flux rate declines gently, whereas gamma radiation exhibits an oscillatory decrease. The presence of polyethylene in the target material was found to have a further reducing effect on both neutron flux and gamma dose rate. In comparison, polyethylene has a more significant impact on the neutron yield, which is consistent with the results of theoretical simulations.

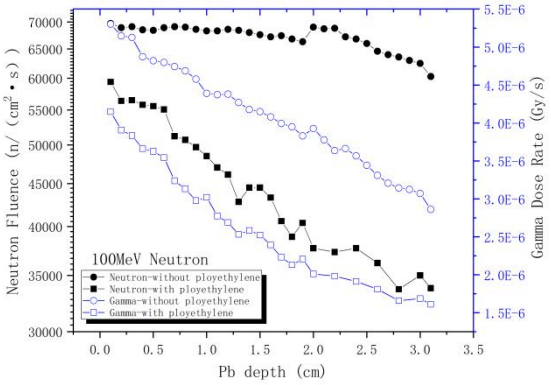

Fig. 7 Neutron Flux and gamma dose rate results after 100 MeV neutrons passing through the regulator

The incident particle was then subjected to 80 MeV proton bombardment of a 4 cm lithium target, with the aim of analyzing the regulator's performance under varying energy input conditions. The results indicate that prior to lead thicknesses of 1.5 cm or less, the trends in neutron and gamma dose changes are similar to those observed under 100 MeV neutron conditions. In cases of thinner lead thickness, there is a tendency for increased neutron injection and gamma dose, which gradually diminish with increased lead thickness in subsequent stages. Especially at the thickness of 1.5 cm, there is a sudden increase in gamma dose rate. The reason for this increase may be analyzed due to beam current instability and the rise in proton flow. The sudden fluctuations in beam intensity prevented the deflection magnet from fully deflecting all protons. Consequently, some protons interacted directly with the modulator or collimator, generating a large amount of secondary gamma rays. To avoid interference caused by the proton flow, the neutron-gamma ratio was chosen as the index for further study.

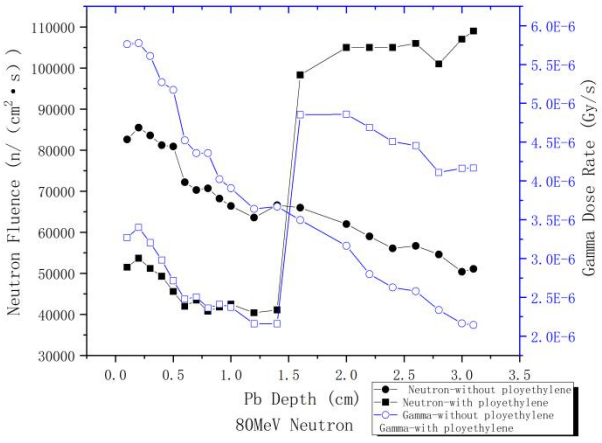

Fig. 8 Neutron flux and gamma dose rate results after 80 MeV neutrons passing through the regulator

4. Discussion

Experimental findings have demonstrated that the neutron gamma ratio can be used as a metric to illustrate influences from the incident proton energy. It has been observed that as the energy of the incident proton increases, the neutron gamma ratio within the generated mixing field decreases.

Upon comparing the neutron-gamma ratio curves under different incident neutron energies, both in the presence and absence of polyethylene, it becomes evident that when the lead thickness is constant, neutron energy significantly influences the regulation of the neutron-gamma ratio. Furthermore, at identical incident neutron energies, the addition of polyethylene further enhances the neutron-gamma ratio. However, the trend observed in modulator thickness is in direct opposition to the theoretical simulation results. That is, in the theoretical simulation model, the addition of polyethylene essentially does not affect the neutron-to-gamma ratio. Instead, it results in a very slight increase.

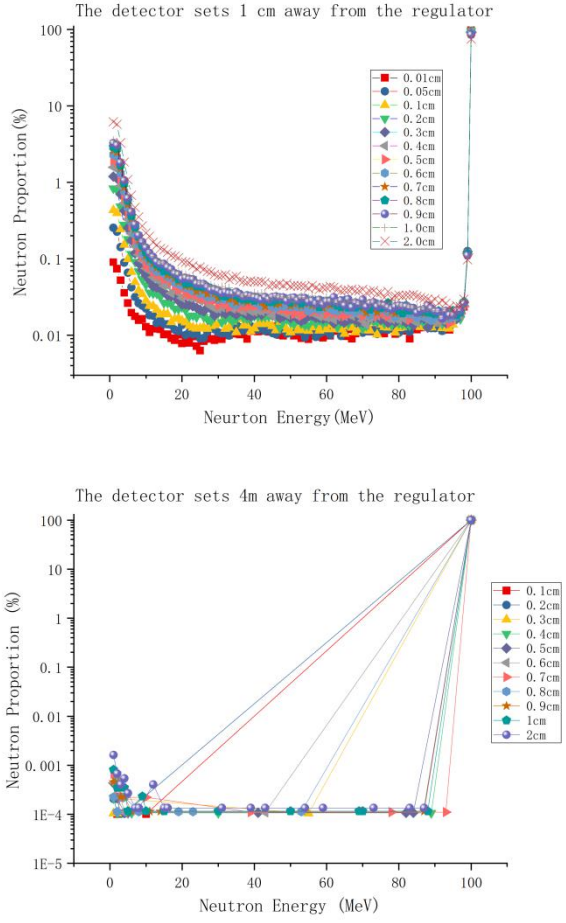

Fig. 9 Normalized neutron detection results after different distances from the detector to the neutron gamma ratio regulator

To analyze the reasons behind the contradictory trends of the theoretical and measured neutron gamma ratios, it was observed that the distance between the detector and the neutron gamma ratio regulator may count. In the theoretical simulation, the distance was relatively close, at just 1 cm. However, considering the collimator, sample bench, and air relaxation distance in actual measurements, the actual detector may be several meters away from the modulator. It is evident that this variation in distance could lead to a significant deviation in the efficiency of neutron detection. To determine the impact of distance on neutron detection, a series of simulations were updated, taking into account the positional variation of the detector. The findings suggest that at a distance of 4 meters, the detected neutrons are primarily of 100 MeV energy, corresponding to the no-loss region. The results indicate that the neutrons detected by the detector at 1 cm are full-energy-spectrum neutrons, whereas beyond a distance of 4 meters, the neutrons detected are predominantly 100 MeV neutrons, and neutrons in the low-energy region are essentially undetected. A comparison analysis of the 100 MeV neutron data from both sets of results show a high degree of consistency between the two detectors. This suggests that the neutrons detected at a distance of 4 meters are predominantly unaltered 100 MeV neutrons, and at this point, the neutron gamma ratio regulator exerts a reduction effect on the neutron yield. It is postulated that the neutrons generated by the proton hitting the target interacted with the primary material of the neutron gamma ratio regulator, resulting in a change in the neutron's trajectory. In the initial 1-cm model, neutron beams in all angular directions were calculated. In experiments, after 0.2 meters of air relaxation, 3 meters of iron collimator collimation, and an additional 0.8 meters of air relaxation, the neutrons with altered angles (colliding neutrons) have exceeded the detection range of the detector, leading to a reduction in the number of detected neutrons.

After calculating the updated model using the FLUKA simulation codes, the theoretical simulation results and measurements results of the neutron-gamma ratio from collision of protons with a lithium target, are presented in Fig.13.

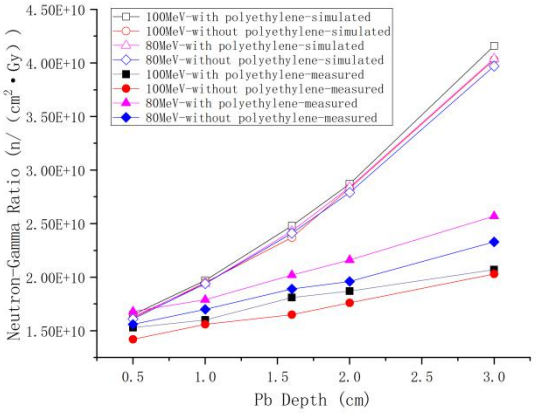

Fig. 10 Theoretical and experimental results of neutron gamma ratio

The trend in theoretical and experimental measurements is consistent when incident energy is 100MeV, yet a significant discrepancy has been observed at 80MeV. The findings suggest that theoretical values closely align with error values for lead thicknesses less than 1 cm. However, the discrepancy between theoretical results and experimental measurements exceeds 30% for lead thicknesses greater than 1.6 cm. Moreover, the error

between theoretical values and experimental values is more pronounced in the absence of polyethylene than in its presence.This indicates that in the high-energy region, the designed modulator essentially meets the anticipated requirements. However, as neutron energy decreases, an increase in certain reaction cross-sections results in greater divergence of the neutron-gamma yield, necessitating an adjustment to the original thickness combination model.

By using the results at a lead thickness of 0.5 cm as a benchmark, the neutron and gamma results were then normalized. It was determined that the theoretical-experimental error in the neutron flux rate was too minimal to ignore, while the primary source of divergence was the theoretical-experimental error of the gamma yield. The deviation of the experimental measurements above the theoretical value reaches 70% at lead thicknesses up to 3 cm. This is primarily due to the fact that the proportion of low-energy neutrons significantly increases under a relatively large lead thickness, with some of these low-energy neutrons reacting with the beam transport device and other environmental equipment to become the primary secondary gamma source. Therefore, it is crucial to optimize the shielding of the beam transport line, with the aim of reducing this part of the secondary gamma rays, thus ensuring that the background gamma value in the environment remains low. This, in turn, will ensure that the neutron gamma ratio at the irradiated sample location is as anticipated.

5. Conclusion

The study elucidated that a neutron-gamma mixed radiation field can be generated by protons hitting a lithium target. The Monte Carlo method was then used to simulate and calculate the change in neutron and gamma yield after neutrons passing through various substances. Considering several factors, lead was selected as the primary material for the neutron-gamma ratio regulator, with polyethylene serving as the auxiliary material. Through analysis of the simulation results, the neutron-gamma ratio regulator's design scheme was determined. The study utilized a binary combination to establish a fixed polyethylene slice for 0.1cm and an adjustment scheme for lead thickness, ranging from 0.1 cm to 3.1 cm, with increments of 0.1 cm. The neutron-gamma field generated by protons hitting the lithium targets was then modulated and measured based on the S1 quasi-monoenergetic neutron branch line at the 100 MeV strong flow proton cyclotron of CIAE, and the model was further optimized. The results indicate that the neutron-gamma ratio regulator can effectively achieve quasi-continuous adjustability of the n-γ ratio, ranging from a few to several hundred, which can effectively meet the needs of various irradiation environments with different neutron-gamma mixed fields. Furthermore, the regulator significantly modifies the angular distribution of secondary particles. Consequently, in practical applications, techniques such as expanding the effective area of the detector, optimizing shielding against secondary gamma rays and stabilizing the incident beam intensity are necessary to stabilize the mixed radiation field, thereby achieving the optimal simulation test conditions.

Acknowledgements

The authors are indebted to the CNNC Basic Research Foundation (CNNC-JCYJ-202313) for financial support, to the 100MeV Strong Flow Proton Cyclotron of CIAE for equipment and experimental technical support, and to Dr. Yihao Gong in particular for his invaluable support for this study.

References

[1] Swinhoe, M.T., Ensslin, N. (2024). The Origin of Neutron Radiation. In: Geist, W.H., Santi, P.A., Swinhoe, M.T. (eds) Nondestructive Assay of Nuclear Materials for Safeguards and Security. Springer, Cham. https://doi.org/10.1007/978-3-031-58277-6_13

[2] Ma, QL., Tang, Sb. , Zou, JW. Numerical simulation of high-energy neutron radiation effect of scintillation fiber[J]. NUCL SCI TECH 19, 004 (2008). https://doi.org/10.1016/S1001-8042(08)60056-1

[3] Verdera, A., Praena, J. Study on novel neutron irradiation without beam shaping assembly in Boron Neutron Capture Therapy. Sci Rep 14, 22434 (2024). https://doi.org/10.1038/s41598-024-73458-w

[4] Roult dit Rouaux, J., Carasco, C., Loubet, L. et al. Experimental gamma coincidence spectra recorded in prompt gamma neutron activation analysis. J Radioanal Nucl Chem 333, 6577 – 6592 (2024). https://doi.org/10.1007/s10967-024-09822-x

[5] Kuzmin, E.S., Bokuchava, G.D., Zimin, I.Y. et al. Comparative Analysis of the Neutron – Gamma Discrimination Methods for Scintillators Based on Lithium Glass. Instrum Exp Tech 67, 234 – 239 (2024). https://doi.org/10.1134/S0020441224700465

[6] Li, JX., Hou, HL., Huang, YF. et al. Pulse-shaping method for real-time neutron/gamma discrimination at low sampling rates. NUCL SCI TECH 34, 165 (2023). https://doi.org/10.1007/s41365-023-01306-z

[7] Zhang, H., Wu, W., Song, X. et al. Novelty in the interpretation of gamma rates recorded by a pulse neutron-gamma probe for gas reservoir determination. J Radioanal Nucl Chem 332, 1825 – 1834 (2023). https://doi.org/10.1007/s10967-023-08848-x

[8] Sangaroon, S., Ogawa, K. & Isobe, M. Neutron emission spectrometer in magnetic confinement fusion. AAPPS Bull. 34, 34 (2024). https://doi.org/10.1007/s43673-024-00139-1

[9] Okajima, S., Kugo, T., Mori, T. (2024). Nuclear Fission and the Neutron Chain Reactions. In: Nuclear Reactor Physics. An Advanced Course in Nuclear Engineering, vol 5. Springer, Tokyo. https://doi.org/10.1007/978-4-431-55600-8_2

[10] Miskevich, A.I. Generation and Quenching in the XeCl* Excimer Laser Pumped by Mixed Gamma-Neutron Radiation from a Nuclear Reactor. Opt. Spectrosc. 132, 391 – 398 (2024). https://doi.org/10.1134/S0030400X2404012X

[11] Yastrebinsky, R.N., Bondarenko, G.G., Pavlenko, V.I. et al. Verifying a Two-Dimensional Model Simulating Attenuation of Neutron and Photon Radiation from Nuclear Reactors Having Metal Hydride Composite Protection. Inorg. Mater. Appl. Res. 15, 319 – 327 (2024). https://doi.org/10.1134/S2075113324020461

[12] Kelly, J.G., Luera, T.F., Posey, L.D. , et al. Simulation fidelity issues in reactor irradiation of electronics-reactor environments[J]. IEEE Transactions on Nuclear Science, 1988, 35:1242-1247

[13] 李俊杰, 邱东, 杜金. 混合辐射场 n、γ 比调节器设计[J]. 核动力工程, 2008, 29:102-105.

[14] Kumada, H., Sakae, T. & Sakurai, H. Current development status of accelerator-based neutron source for boron neutron capture therapy. EPJ Techn Instrum 10, 18 (2023). https://doi.org/10.1140/epjti/s40485-023-00105-5

[15] Kang, S., Kim, J., Kim, J.H. et al. Neutron irradiation facilities, neutron measurement system, and mono-energetic neutron fields at KRISS. J. Korean Phys. Soc. 82, 586 – 594 (2023). https://doi.org/10.1007/s40042-023-00713-0
[16] Berry, K.D., Diawara, Y. (2023). Neutron Detection Materials, Detector Properties, and Selection. In: Diawara, Y. (eds) Neutron Detectors for Scattering Applications. Particle Acceleration and Detection. Springer, Cham. https://doi.org/10.1007/978-3-031-36546-1_2
[17] Wang, XY., Chen, JY. & Zhang, Q. Boron shielding design for neutron and gamma detectors of a pulsed neutron tool. NUCL SCI TECH 36, 16 (2025). https://doi.org/10.1007/s41365-024-01605-z
[18] Tang, E. S., Yan, Y. L., Xia, S. J., et al. New wiggler beamlines at BSRF. Journal of synchrotron radiation, 5, 530-532 (1998). https://doi.org/10.1107/S0909049597014763
[19] Liu, XY., Yang, YW., Liu, R. et al. Measurement of the neutron total cross section of carbon at the Back-n white neutron beam of CSNS. NUCL SCI TECH 30, 139 (2019). https://doi.org/10.1007/s41365-019-0660-9
[20] Xu, J., Cheng, W., Jia, W. et al. Neutron-gamma pulse shape discrimination for EJ301 liquid scintillator based on machine learning. J Radioanal Nucl Chem 333, 905 – 916 (2024). https://doi.org/10.1007/s10967-023-09327-z
[21] Wang, R. S., Ou, L., & Xiao, Z. G. Production of high - energy neutron beam from deuteron breakup. NUCL SCI TECH 33, 92 (2022). https://doi.org/10.1007/s41365-022-01075-1
[22] Malidarre, R.B., Akkurt, I. Simulation of neutron and gamma radiation shielding properties of KNN-LMN lead-free relaxor ceramics. J Aust Ceram Soc 59, 137 – 143 (2023). https://doi.org/10.1007/s41779-022-00819-x
[23] Tang, W., Liang, JG., Ge, Y. et al. A method for neutron-induced gamma spectra decomposition analysis based on Geant4 simulation. NUCL SCI TECH 33, 154 (2022). https://doi.org/10.1007/s41365-022-01144-5
[24] Zayed, A.M., El-Khayatt, A.M., Mahmoud, K.A. et al. Evaluation of Some Heavyweight Minerals as Sustainable Neutron and Gamma-Ray Attenuating Materials: Comprehensive Theoretical and Simulation Investigations. Arab J Sci Eng (2024). https://doi.org/10.1007/s13369-024-09300-2
[25] Hosseini Sarteshnizi, H., Eshghi, M. Gamma ray and neutron shielding capacity of and dosimetry of composite compounds with diagnostic and therapeutic energies. Radiat Detect Technol Methods 8, 1217 – 1228 (2024). https://doi.org/10.1007/s41605-023-00438-5